

IRAM- Ω -Q: A Computational Architecture for Uncertainty Regulation in Artificial Agents

Veronique Ziegler
Independent Researcher
[upsilon3s@gmail.com]

Abstract

Artificial agents can achieve strong task performance while remaining opaque with respect to internal regulation, uncertainty management, and stability under stochastic perturbation. We present IRAM- Ω -Q, a computational architecture that models internal regulation as closed-loop control over a quantum-like state representation. The framework uses density matrices instrumentally as abstract state descriptors, enabling direct computation of entropy, purity, and coherence-related metrics without invoking physical quantum processes. A central adaptive gain is updated continuously to maintain a target uncertainty regime under noise.

Using systematic parameter sweeps, fixed-seed publication-mode simulations, and susceptibility-based phase-diagram analysis, we identify reproducible critical boundaries in regulation–noise space. We further show that alternative control update orderings, interpreted as perception-first and action-first architectures, induce distinct stability regimes under identical external conditions. These results support uncertainty regulation as a concrete architectural principle for artificial agents and provide a formal setting for studying stability, control, and order effects in cognitively inspired AI systems.

The framework is presented as a technical model of adaptive regulation dynamics in artificial agents. It makes no claims regarding phenomenological consciousness, and the quantum-like formalism is used strictly as a mathematical representation for structured uncertainty and state evolution.

1 Introduction

Artificial intelligence systems have achieved remarkable task performance, yet remain largely opaque with respect to internal regulation, stability, and uncertainty control. Classical symbolic architectures emphasize explicit structure but often degrade under stochastic perturbation, while end-to-end learning systems can exhibit robustness without transparent internal control mechanisms. This creates a modeling gap for architectures that can both represent internal state structure and regulate that structure online under noise.

Quantum-like approaches to cognition offer one useful mathematical toolkit for addressing this gap. Hilbert-space representations and density matrices can encode contextuality (the dependence of outcome probabilities on measurement context, including order and compatibility relations among observables), graded uncertainty, and ordering effects in decision-making and perception [5]. However, most such models remain open-loop: uncertainty is analyzed as an outcome of dynamics rather than treated as a quantity that the system actively regulates.

We introduce IRAM- Ω -Q (Integrated Regulation and Attention Model with Ω -regulation and Quantum-like state representation), a computational architecture for studying adaptive cognitive

regulation in artificial agents. Here, the symbol Ω denotes the explicit adaptive regulation component of the architecture. The framework is designed to investigate how agents maintain coherence, stability, and identity persistence under stochastic perturbation through closed-loop internal control.

In this framework, cognitive regulation is modeled as adaptive control over the evolution of a *quantum-like* state representation in Hilbert space, using density matrices as an instrumental, information-theoretic descriptor [5]. Unlike open-loop formulations, the present architecture embeds a feedback mechanism that dynamically adjusts an internal regulation gain to maintain a target uncertainty regime under noise.

The contribution is architectural rather than metaphysical. IRAM- Ω -Q provides operational definitions and measurable quantities aligned with cognitive systems, adaptive control, and uncertainty-aware AI. It makes no claims regarding phenomenological consciousness or physical quantum processes.

Contribution Summary: This work makes three primary contributions.

- First, we introduce a closed-loop adaptive regulation mechanism within a quantum-like cognitive state model, allowing uncertainty—quantified via von Neumann entropy—to be actively controlled rather than passively observed.
- Second, we apply a systematic phase-diagram methodology to adaptive cognitive regulation, identifying critical boundaries in regulation–noise space via susceptibility analysis.
- Third, we demonstrate that alternative control orderings, interpreted as perception-first and action-first architectures, induce systematic shifts in adaptive stability.

Together, these contributions establish adaptive entropy regulation as a computational principle linking formal state modeling, uncertainty control, and algorithmic architecture design.

To avoid conceptual ambiguity, we emphasize that terms such as “awareness” and “attention” are used strictly in an operational, control-theoretic sense throughout this work. They refer to the capacity of a dynamical system to monitor and regulate internal uncertainty through closed-loop feedback and to allocate regulatory gain within the update dynamics. No claims are made regarding phenomenology, subjective experience, or self-modeling. The framework is therefore best understood as a formal study of adaptive regulation dynamics in artificial agents rather than a theory of consciousness.

2 Conceptual Framework

2.1 Adaptive Cognitive Regulation

In IRAM- Ω -Q, adaptive cognitive regulation is treated as a control-theoretic process: the system monitors internal uncertainty and dynamically adjusts regulatory parameters to preserve global integration. Within this framework, “attention” is defined operationally as the allocation of regulatory gain within the state-update dynamics under stochastic perturbation. The adaptive parameter μ functions as a global regulatory resource, modulating the relative contribution of the regulation-modulated generator and the stochastic term in the evolution equation. Stable regulation therefore emerges as a dynamical regime maintained by closed-loop feedback rather than as an explicit symbolic representation. Although the current implementation employs a scalar gain, the formalism

naturally extends to component-wise or stimulus-specific regulation, permitting competing stimulus selection, salience weighting, and bottleneck-like dynamics in future extensions.

2.2 Order-Dependent Perception–Action Coupling

A central design feature is the explicit distinction between two update orderings:

- **Perception-first (PF)**: perceptual integration precedes control modulation and action.
- **Action-first (AF)**: control modulation and action precede perceptual integration.

While often treated as an implementation detail, in this work update ordering is shown to induce qualitatively distinct dynamical regimes under identical parameter settings. Importantly, these are *control orderings* (architectural interventions), and not measurement-order effects in the quantum-cognition sense.

3 Architecture

3.1 State Representation

Cognitive state is represented using a density matrix $\rho(t)$ evolving under open-system-like dynamics:

$$\frac{d\rho}{dt} = -i[H(\mu), \rho] + \mathcal{D}(\rho), \quad (1)$$

where $H(\mu)$ is a regulation-modulated effective generator governing state integration dynamics, and \mathcal{D} is a noise-induced dissipative term representing stochastic environmental perturbations. The adaptive gain μ scales the strength of the integrative component encoded in $H(\mu)$.

This representation enables direct computation of entropy, purity, and coherence-related metrics using standard mathematical definitions, without invoking physical quantum processes.

3.2 Control Architecture and Adaptive Regulation

The scalar parameter μ acts as an *internal regulation gain* controlling the balance between perceptual integration—defined here as the consolidation of incoming stochastic perturbations into the current state representation—and action commitment, defined as the stabilization and propagation of the updated state into subsequent dynamics. Operationally, μ scales the contribution of the regulation-modulated generator $H(\mu)$ relative to stochastic perturbation in the state-update equation, thereby determining how aggressively the system suppresses entropy growth prior to state propagation. The gain μ is updated via closed-loop feedback proportional to deviations from the target entropy regime. Increases in entropy or coherence gap induce increases in μ , thereby increasing the relative contribution of the regulation-modulated generator $H(\mu)$ compared to the stochastic perturbation term $\mathcal{D}(\rho)$ in the state-update equation. When entropy remains within the target regime, the update term diminishes, allowing μ to converge toward a stable fixed point.

Low values of μ correspond to underregulated dynamics dominated by external perturbations, while intermediate values promote stable integration. At high values, regulatory effectiveness saturates, yielding diminishing returns rather than runaway control.

4 Metrics and Observables

The framework tracks global observables, including:

- von Neumann entropy
- coherence gap
- control signal evolution $\mu(t)$
- stability and susceptibility indicators

4.1 Coherence Gap

For a density matrix $\rho(t)$, we define the coherence gap as

$$\Delta C(t) = 1 - \text{Tr}(\rho(t)^2). \quad (2)$$

The coherence gap provides a bounded, dimensionless measure of global state fragmentation. $\Delta C = 0$ corresponds to a maximally pure (fully integrated) state within the representation, while larger values indicate increasing mixedness/fragmentation. Time-averaged coherence gap values serve as the primary order parameter in phase-diagram analysis.

5 Experimental Methods

All publication-mode figures were generated using fixed random seeds, identical burn-in windows, and frozen simulation parameters to ensure exact reproducibility.

5.1 Exploratory vs. Publication Analysis Modes

To ensure methodological rigor, IRAM- Ω -Q distinguishes between two analysis modes. **Exploratory mode** is used for rapid hypothesis development and qualitative inspection. In this mode, parameter sweeps are computed with minimal averaging and without burn-in enforcement. Results from exploratory mode are not used to support formal claims.

Publication mode enforces fixed burn-in windows, multi-run averaging, and susceptibility tracking. Only publication-mode results are reported in figures and quantitative analysis. This separation prevents exploratory bias from contaminating reported regime structure.

5.2 Simulation Protocol

Experiments consist of repeated stochastic simulations sweeping over:

- initial regulatory gain μ
- environmental noise amplitude η
- perception–action update ordering

Each simulation discards an initial burn-in window before metrics are collected, ensuring transient dynamics do not influence reported values.

5.3 Phase Diagram Computation

Phase diagrams are constructed by sweeping (μ, η) over a fixed grid. For each grid point, multiple independent runs are performed. The coherence gap is computed at each time step, averaged over the post-burn-in window, and then averaged across runs. This procedure is implemented in the `PhaseDiagramSweep` class.

5.4 Adaptive Control Dynamics and Stability Diagnostics

In addition to tracking the regulatory gain $\mu(t)$, the framework records its incremental update

$$\Delta\mu(t) = \mu(t) - \mu(t - \Delta t), \quad (3)$$

which serves as a direct diagnostic of control activity and stability. Convergence of $\Delta\mu(t)$ toward zero indicates that the regulatory loop has reached a fixed point, while sustained oscillations or divergence would signal instability. In all reported publication-mode experiments, $\Delta\mu(t)$ exhibits transient excursions followed by bounded fluctuations around zero, consistent with convergence to a stable regulation fixed point.

5.5 Operational Definition of Critical Boundaries

Critical boundaries are defined via peaks in susceptibility of global metrics. For coherence gap ΔC , we define a susceptibility proxy as the post-burn-in temporal variance

$$\chi(\mu, \eta) = \text{Var}_{t \in [T_1, T_2]}[\Delta C(t)]. \quad (4)$$

For each noise level η , an estimated critical control value is identified as

$$\hat{\mu}_c(\eta) = \arg \max_{\mu} \chi(\mu, \eta). \quad (5)$$

This provides a reproducible criterion for identifying regime boundaries without invoking thermodynamic criticality.

We note that the critical boundary $\hat{\mu}_c(\eta)$ identified here is an estimator-dependent regime boundary derived from finite-time susceptibility peaks. It is not claimed to represent a mathematically proven bifurcation of the underlying infinite-time dynamical system. The term “phase” is therefore used in an operational, dynamical-systems sense to denote reproducible regime structure within the simulation framework.

Throughout, $\hat{\mu}_c(\eta)$ denotes the finite-sample critical boundary inferred from susceptibility peaks, and $\bar{\mu}_c$ denotes the noise-averaged mean of $\hat{\mu}_c(\eta)$ across the sampled noise levels.

5.6 Implementation–Metric Correspondence

To ensure reproducibility and methodological transparency, all theoretical quantities introduced in this framework are mapped directly to concrete software components in the IRAM- Ω -Q implementation. Each observable corresponds to a specific Java class or method responsible for its computation, aggregation, or control. Table 1 summarizes the mapping between theoretical concepts, their mathematical definitions, and the corresponding Java implementation.

Table 1: Mapping between theoretical quantities, mathematical definitions, and Java implementation in IRAM- Ω -Q.

| Concept | Mathematical Definition | Java Class / Method |
|------------------|---|--|
| Cognitive state | Density matrix $\rho(t)$ | <code>DensityMatrix</code> |
| Entropy | $S(\rho) = -\text{Tr}(\rho \log \rho)$ | <code>EntropyMetric.compute()</code> |
| Purity | $\text{Tr}(\rho^2)$ | <code>DensityMatrix.purity()</code> |
| Coherence gap | $\Delta C = 1 - \text{Tr}(\rho^2)$ | <code>CoherenceGapMetric.compute()</code> |
| Regulatory gain | Adaptive control parameter $\mu(t)$ | <code>AdaptiveController.updateMu()</code> |
| Noise amplitude | External perturbation η | <code>NoiseModel.apply()</code> |
| Susceptibility | $\chi = \text{Var}_t[\Delta C(t)]$ | <code>SusceptibilityMetric.compute()</code> |
| Critical control | $\hat{\mu}_c = \arg \max_{\mu} \chi(\mu, \eta)$ | <code>PhaseDiagramAnalyzer.detectCriticalMu()</code> |
| Phase diagram | Grid over (μ, η) | <code>PhaseDiagramSweep.run()</code> |
| Averaging | $\langle \cdot \rangle_{\text{runs}}$ | <code>AveragedResult</code> |
| Analysis mode | Exploratory vs Publication | <code>AnalysisMode</code> enum |

6 Results

6.1 Definition of the critical regulation threshold

We define a noise-dependent estimated critical regulation threshold $\widehat{\mu}_c(\eta)$ operationally as the regulation gain at which susceptibility with respect to μ is maximal at fixed noise. For each η , simulations are run across a sweep of μ and the susceptibility proxy $\chi(\mu, \eta) = \text{Var}_t[\Delta C(t)]$ is computed over the post-burn-in window. The critical value $\widehat{\mu}_c(\eta)$ is then identified via

$$\widehat{\mu}_c(\eta) = \arg \max_{\mu} \chi(\mu, \eta). \quad (6)$$

We emphasize that $\widehat{\mu}_c(\eta)$ is an *operational* threshold for this architecture and estimator, defined by sensitivity of the closed-loop adaptation, rather than a universal constant.

For summary statistics across noise conditions, we additionally report the noise-averaged critical gain

$$\bar{\mu}_c = \langle \widehat{\mu}_c(\eta) \rangle_{\eta}, \quad \sigma_{\mu_c} = \sqrt{\langle (\widehat{\mu}_c(\eta) - \bar{\mu}_c)^2 \rangle_{\eta}}, \quad (7)$$

which are visualized as vertical markers and uncertainty bands in the phase diagrams.

6.2 Adaptive regulation stabilizes cognitive dynamics

Figure 1 shows representative publication-mode trajectories for von Neumann entropy $S_{vN}(t)$, coherence gap $\Delta C(t)$, regulation gain $\mu(t)$, and adaptive update $\Delta\mu(t)$ under low environmental noise ($\eta = 0.13$; PF). Entropy approaches the target regime while the coherence gap decreases concurrently, indicating suppression of global fragmentation. The adaptive update $\Delta\mu(t)$ converges toward zero in expectation after burn-in, consistent with closed-loop stabilization.

6.3 Robustness across noise regimes

Figure 2 shows the same observables under high noise ($\eta = 0.95$; PF). Although fluctuations increase and higher steady-state regulation is required, entropy and coherence remain bounded and $\Delta\mu(t)$ again converges toward zero in expectation, indicating robust regulation. Importantly, the convergence of $\Delta\mu(t)$ occurs strictly below the imposed upper bound μ_{\max} , indicating genuine stabilization of the adaptive feedback loop rather than saturation at a clipping constraint.

6.4 Phase structure and critical regulation threshold

Figure 3 presents the (μ, η) phase diagram under perception-first ordering. Critical boundaries are identified via susceptibility peaks, yielding an estimated critical curve $\widehat{\mu}_c(\eta)$.

6.5 Effect of perception–action ordering

Two control orderings are compared. In perception-first (PF) ordering, perceptual state integration precedes regulatory action within each update cycle, allowing control to respond to consolidated uncertainty. In action-first (AF) ordering, regulation is applied prior to perceptual consolidation, effectively acting on noisier internal estimates.

As shown in Fig. 4, AF ordering systematically shifts the critical boundary toward higher μ relative to PF ordering. This indicates that acting before perception increases regulatory demand and reduces efficiency. While individual time-course trajectories may appear similar at fixed parameters, sweep-based phase analysis reveals a robust, ordering-dependent shift in $\widehat{\mu}_c(\eta)$.

Table 2: **Simulation parameters used across figures.** Global defaults apply to all figures unless explicitly overridden. All simulations use a fixed base seed for reproducibility (`baseSeed = 123456789`), with per-run seeds `seed = baseSeed + r`, where r indexes stochastic replicates.

| Category | Parameter | Value |
|--------------------------------------|----------------------------|---|
| <i>Global defaults (all figures)</i> | | |
| Time | Steps | 10,000 (publication), 4,000 (fast mode) |
| | Δt | 0.01 |
| State | Dimension | 16 |
| | Saliency center / width | 6.0/2.0 |
| | Phase noise | 0.2 |
| Hamiltonian | Energy scale | 0.15 |
| | Coupling | 0.08 |
| | Locality | 2.0 |
| Control | Target entropy S^* | 0.30 |
| | Learning rate α_μ | 2×10^{-4} |
| | μ_{\min}, μ_{\max} | $10^{-3}, 1.0$ |
| <i>Figure-specific overrides</i> | | |
| Fig. 1 | Ordering | Perception-first (PF) |
| | Noise η | 0.13 |
| | Initial gain μ_0 | 0.08 |
| Fig. 2 | Ordering | Perception-first (PF) |
| | Noise η | 0.95 |
| | Initial gain μ_0 | 0.08 |
| Fig. 3 | Ordering | Perception-first (PF) |
| | Sweep | $\mu \in [0.05, 1.0], \eta \in [10^{-4}, 0.30]$ |
| | Grid resolution | 20×20 (fast), 40×40 (publication) |
| | Runs per point | 5 (fast), 15 (publication) |
| Fig. 4 | Ordering | Action-first (AF) |
| | Sweep | Same as Fig. 3 |

7 Discussion

Unlike free-energy-based formulations that interpret stability in terms of variational inference or generative model optimization [2], the present framework treats uncertainty itself as a directly regulated control variable within a closed-loop dynamical system.

The results demonstrate that closed-loop adaptive regulation is sufficient to generate stable, bounded cognitive-state dynamics across wide noise regimes. The emergence of a well-defined critical boundary $\hat{\mu}_c(\eta)$ is consistent with a phase-transition-like *regime structure* in the operational, susceptibility-defined sense used here separating under-regulated and self-stabilizing regimes, defined operationally via susceptibility peaks. This structure is observed reproducibly across entropy, coherence, and adaptive-gain diagnostics.

The distinction between perception-first and action-first control ordering highlights the importance of temporal structure in adaptive regulation. While single-run trajectories can mask these effects, sweep-based phase analysis reveals systematic and reproducible differences, underscoring

the need for population-level evaluation of adaptive cognitive architectures.

7.1 Limitations

The present study focuses on a single-agent architecture and finite simulation horizons. While adaptive stability is consistently observed, longer runs and multi-agent extensions may reveal additional dynamical regimes. Furthermore, the density-matrix formalism is used instrumentally and does not capture representational content, task semantics, or reward-driven learning.

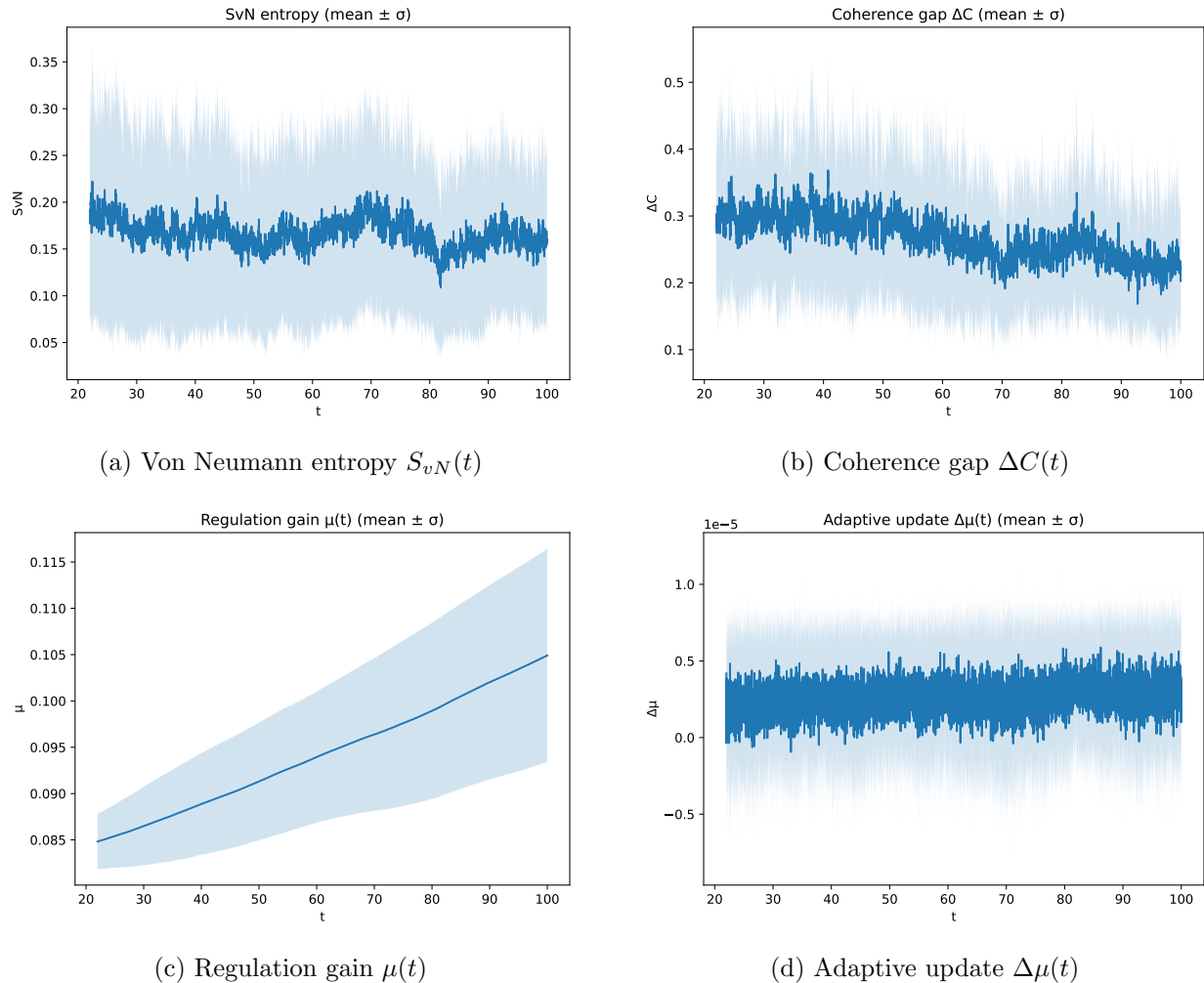
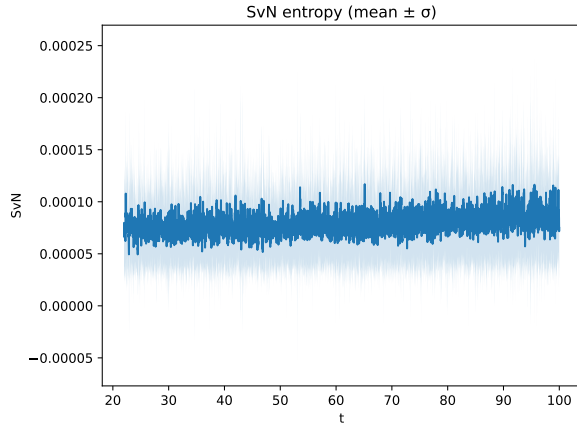
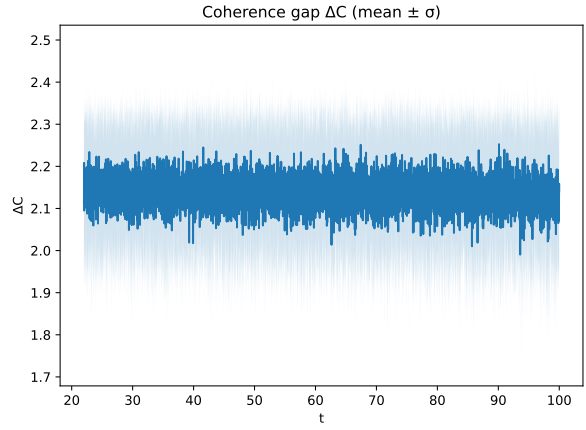


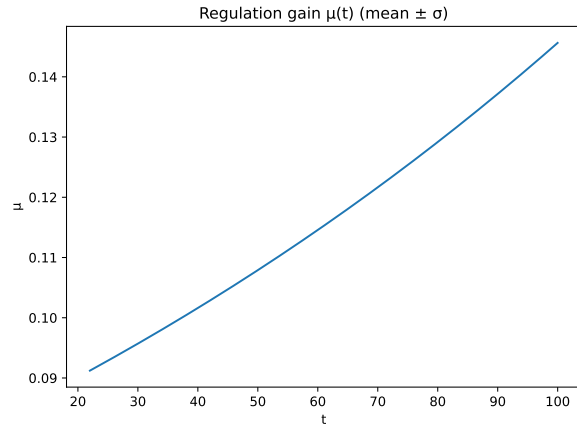
Figure 1: **Time-course dynamics under low noise ($\eta = 0.13$; perception-first ordering).** Panels show $S_{vN}(t)$, $\Delta C(t)$, $\mu(t)$, and $\Delta\mu(t)$ (mean $\pm 1\sigma$ across independent seeds; shaded bands). After burn-in, $\Delta\mu(t)$ fluctuates around zero and the mean update converges, indicating closed-loop stabilization rather than monotonic drift.



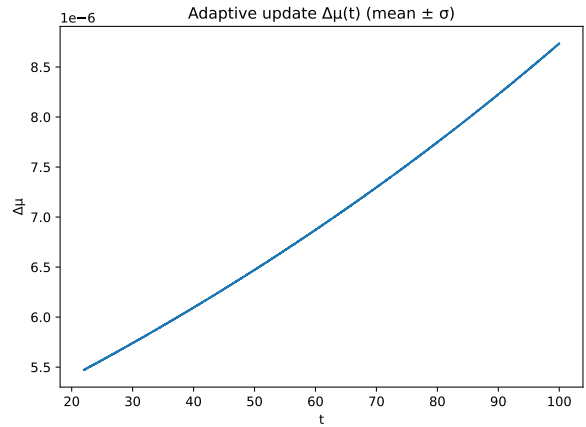
(a) Von Neumann entropy $S_{vN}(t)$



(b) Coherence gap $\Delta C(t)$



(c) Regulation gain $\mu(t)$



(d) Adaptive update $\Delta\mu(t)$

Figure 2: **Time-course dynamics under high noise ($\eta = 0.95$; perception-first ordering).** Despite stronger fluctuations, $S_{vN}(t)$ and $\Delta C(t)$ remain bounded and the adaptive update $\Delta\mu(t)$ converges toward zero in expectation (mean $\pm 1\sigma$ across seeds). The convergence occurs strictly below the imposed upper bound μ_{max} , indicating stabilization rather than saturation at the clipping constraint. This demonstrates that stability is not restricted to low-noise conditions and does not depend on a single favorable random initialization.

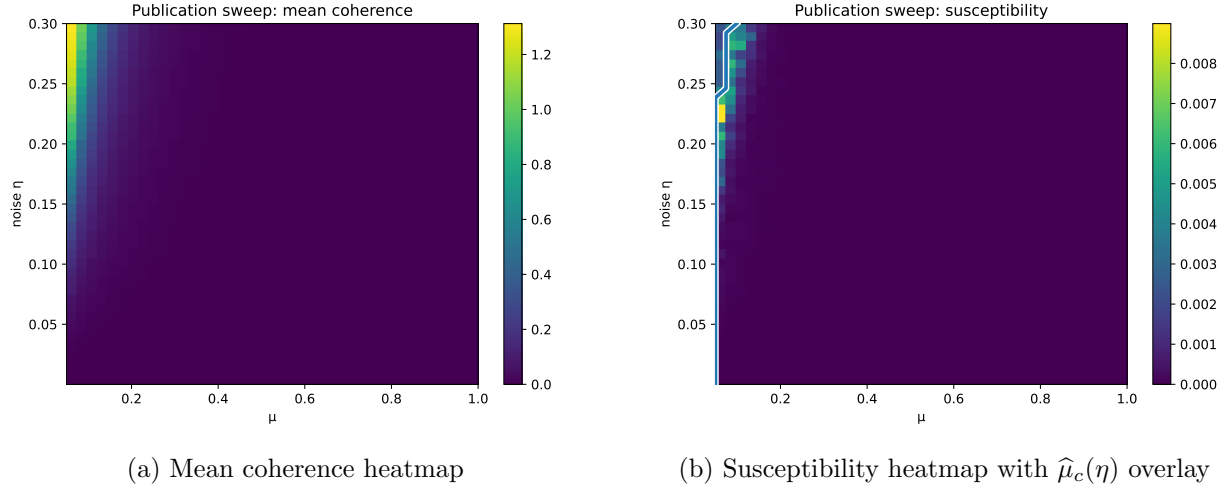


Figure 3: **Publication-mode phase diagram (perception-first ordering)**. Left: mean coherence gap over the (μ, η) grid (post-burn-in average, then averaged across runs). Right: susceptibility proxy $\chi(\mu, \eta)$ with the detected critical curve $\hat{\mu}_c(\eta)$ overlaid (defined by the μ -argmax of χ at fixed η).

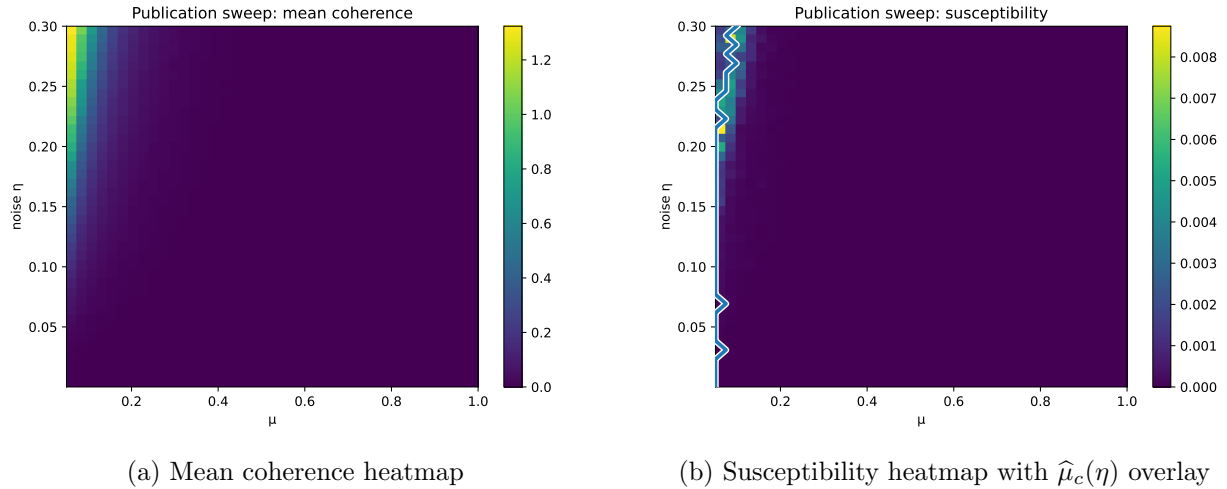


Figure 4: **Publication-mode phase diagram (action-first ordering)**. Left: mean coherence gap over the (μ, η) grid. Right: susceptibility proxy with detected $\hat{\mu}_c(\eta)$ overlay. Relative to Fig. 3, the regulated regime is shifted toward higher μ , indicating increased regulatory demand when control precedes perceptual consolidation.

Supplementary: Robustness Analysis

All supplemental figures are generated from frozen configuration files using the same simulation pipeline as the main text, and are intended to assess robustness to random seeds, analysis windows, and observable definitions.

We performed additional robustness tests to verify that the observed critical behavior is not an artifact of numerical or stochastic choices. Specifically, we varied:

- (i) random seed,
- (ii) simulation horizon,
- (iii) μ -grid resolution,
- (iv) post-burn-in window choices, and
- (v) control ordering (PF vs. AF).

Across all tests, the qualitative structure of the phase diagram and the ordering of regimes were preserved. While individual realizations exhibit small fluctuations in the estimated $\hat{\mu}_c(\eta)$, ensemble-averaged values $\bar{\mu}_c$ converge rapidly with increasing sample size. These results confirm that the regime boundary reflects a structural property of the adaptive dynamics.

Supplementary Appendix: Robustness and Estimation Details

S1. Operational estimator for the critical threshold $\hat{\mu}_c(\eta)$

For each fixed noise level η , we sweep the regulation gain μ over a grid $\{\mu_1, \dots, \mu_M\}$ and compute the susceptibility proxy $\chi(\mu, \eta) = \text{Var}_{t \in [T_1, T_2]}[\Delta C(t)]$ after burn-in. We define the critical threshold as the maximizer of the empirical susceptibility,

$$\hat{\mu}_c(\eta) \equiv \arg \max_{\mu_k} \hat{\chi}(\mu_k, \eta). \quad (8)$$

Noise-averaged summary. Across a discrete set of noise levels $\{\eta_1, \dots, \eta_N\}$, we report

$$\bar{\mu}_c \equiv \frac{1}{N} \sum_{j=1}^N \hat{\mu}_c(\eta_j), \quad \sigma_{\mu_c} \equiv \sqrt{\frac{1}{N-1} \sum_{j=1}^N (\hat{\mu}_c(\eta_j) - \bar{\mu}_c)^2}. \quad (9)$$

In phase diagrams, we visualize the full curve $\hat{\mu}_c(\eta)$ and the summary statistic $\bar{\mu}_c \pm \sigma_{\mu_c}$.

A Reproducibility

All results and figures are reproducible from deterministic, headless command-line runs of the IRAM- Ω -Q codebase. Each figure is generated from a dedicated configuration file (stored under `paper/configs/`) that specifies model parameters, control ordering, grid definitions (for sweeps), random seed(s), burn-in, and number of runs per condition. Every execution writes an immutable record of the run settings (`run.properties`) and a provenance log (`manifest.txt`) into the corresponding output directory under `paper/runs/`, alongside raw numerical outputs (CSV). Canonical plotting scripts (under `paper/scripts/`) transform these CSV outputs into paper-ready figure PDFs (under `paper/`) without manual editing.

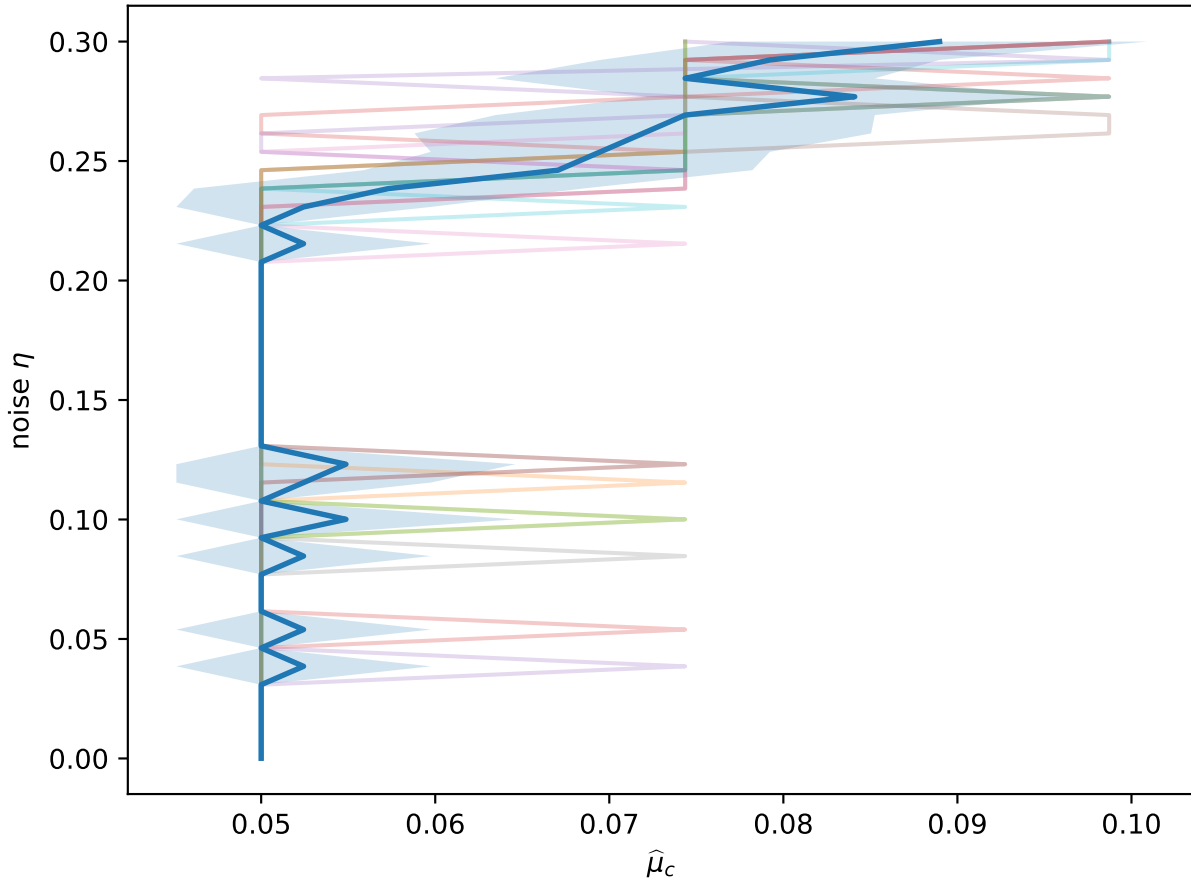


Figure 5: **Seed robustness of the critical curve $\hat{\mu}_c(\eta)$ (perception-first ordering).** The complete sweep is repeated across independent random seeds. Thin curves show $\hat{\mu}_c(\eta)$ per seed; the thick curve shows the across-seed mean, and the shaded region denotes $\pm 1\sigma$ across seeds.

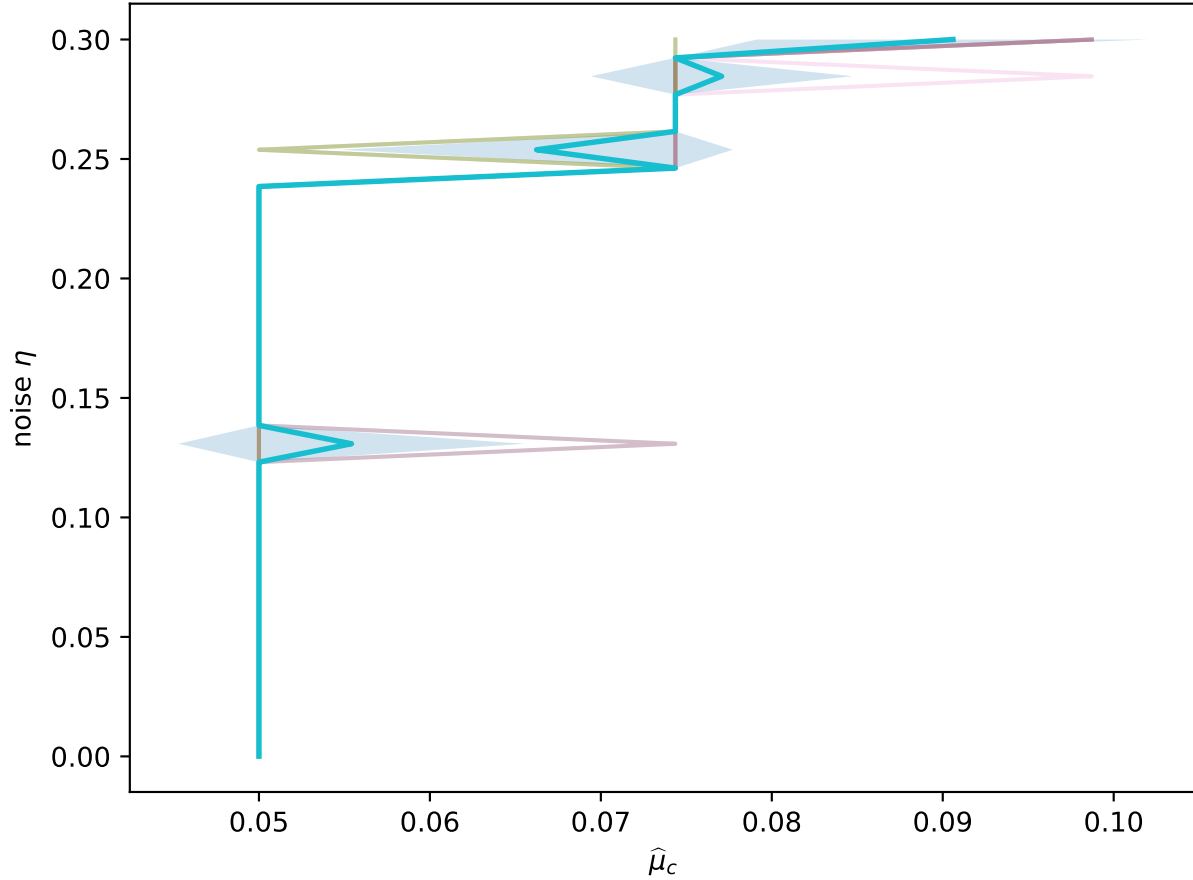


Figure 6: **Robustness of $\hat{\mu}_c(\eta)$ to post-burn-in window choices (perception-first ordering)**. We recomputed $\hat{\mu}_c(\eta)$ while varying burn-in and averaging window length. Curves show resulting thresholds; the envelope across window choices remains narrow relative to ordering-dependent shifts in the main text.

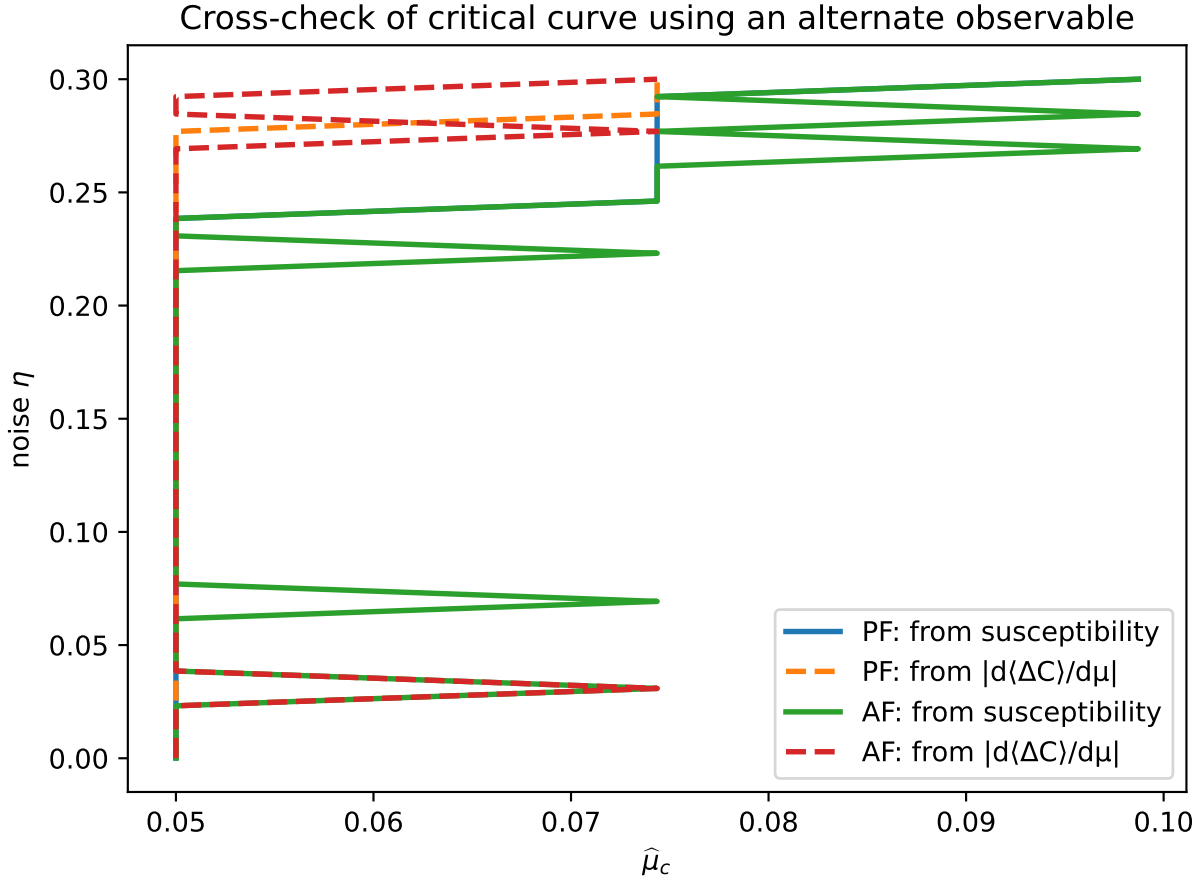


Figure 7: **Metric cross-check for the regime boundary.** Critical boundaries estimated from independent observables agree qualitatively and yield similar $\hat{\mu}_c(\eta)$ trends, supporting the interpretation that the phase structure reflects a system-level regime change rather than a single-metric artifact.

References

- [1] G. Tononi, “An information integration theory of consciousness,” *BMC Neuroscience*, 2004.
- [2] K. Friston, “The free-energy principle: a unified brain theory?,” *Nature Reviews Neuroscience*, 2010.
- [3] K. J. Åström and R. M. Murray, *Feedback Systems*, Princeton University Press, 2008.
- [4] S. Bedau et al., “Open problems in artificial life,” *Artificial Life*, 2000.
- [5] J. R. Busemeyer and P. D. Bruza, *Quantum Models of Cognition and Decision*, Cambridge University Press, 2012.
- [6] M. Asano, I. Basieva, A. Khrennikov, M. Ohya, and Y. Tanaka, “Quantum-like dynamics of decision-making,” *Physica A: Statistical Mechanics and its Applications*, 391(5):2083–2099, 2012.
- [7] E. Tognoli and J. A. S. Kelso, “The metastable brain,” *Neuron*, 81(1):35–48, 2014.